25th ABCM International Congress of Mechanical Engineering
October 20-25, 2019, Uberlândia, MG, Brazil

COB-2019-2026
PURE ELASTIC INSTABILITY OF WORMLIKE MICELLES FLOW IN A CROSS-SLOT

Francisco de Souza Forte Neto
Antônio Guilherme Barbosa da Cruz
Faculty of Mechanical Engineering, ITEC, Federal University of Pará, Belém, PA, Brazil
fforteneto@gmail.com
aguicruz@ufpa.br

Abstract. *This work presents a numerical study of the elastic instability in a surfactant micellar solution when flowing through a cross-slot bifurcation. The elastic instability is characterized by the break of the symmetry of the flow. We adopt the two species VCM model for the wormlike micelles evolution in the flow. The model was implemented and solved in the finite element software COMSOL Multiphysics. Numerical simulations show that the symmetry breakage of the flow due to the elastic instability in micellar solutions occurs for a critical Deborah number. Further, we verify the influence of a source/sink terms presented in the balance equations for the number density of the chains, which have a strong influence on the total number density of the chains. This suggests that it should not be neglected in this type of analysis.*

Keywords: *Elastic instability, wormlike micelles, cross-slot bifurcation, finite elements*

1. INTRODUCTION

Under certain flow conditions, wormlike micellar solutions can exhibit peculiar behavior. For example, temporary structures formation, shear banding, and shear thickening (Dubash *et al.*, 2012). In extensional flow, as in a cross-slot geometry, wormlike micellar solutions exhibit elastic instabilities that induce symmetry breaking in the flow field. The understanding of this phenomenon has been extensively investigated experimentally (Haward *et al.*, 2012; Haward and McKinley, 2012; Dubash *et al.*, 2012) and through numerical simulations (see, e.g., Kalb *et al.* (2017, 2018)).

Recently, Kalb *et al.* (2017) and Kalb *et al.* (2018) studied the elastic instability and secondary flow in cross-slot flows of wormlike micellar solutions using a two species model, the so-called VCM model, that account the breakage and reforming of the micelle chains. In their analysis, however, they have neglected terms that arise in the diffusion concentration of the chains due to the finite length of the micellar chains. In particular, the multiple species model VCM (Vasquez *et al.*, 2007) has an advantage over other models, since it can be directly related to the microstructure and the breakage and reforming of the micellar chains (Kalb *et al.*, 2018).

In this work, we use a complete version of the VCM model to investigate the onset of purely elastic instabilities in wormlike micellar flows in which the rheology of the micellar solution predicts only shear and extensional thinning, avoiding the formation of shear banding. The VCM model was implemented and solved in the finite element software COMSOL *Multiphysics*. Through the simulations, we verified the flow symmetry breakage caused by the phenomenon of the elastic instability in micellar solutions for a localized critical Deborah number.

Numerical simulations show that the symmetry breakage of the flow due to the elastic instability in micellar solutions occurs for a critical Deborah number. Further, we verify the influence of a source/sink terms presented in the balance equations for the number density of the chains, which have a strong influence on the total number density of the chains. This suggests that it should not be neglected in this type of analysis.

2. RHEOLOGICAL MODEL

We adopt the VCM model (Vasquez *et al.*, 2007) for wormlike micellar solutions. The model considers the existence of two chains species in which a long chain can break and form short chains and they can reconnect and form a long chain. The dimensionless evolution equations of the VCM model are given by

$$\mu\left(\frac{\partial n_A}{\partial t}+\mathbf{u}\cdot\nabla n_A\right)-\nabla\cdot\left(\delta_A\left(2\nabla n_A-\nabla\cdot\mathbf{A}\right)\right)=\frac{1}{2}c_B n_B^2-c_A n_A, \tag{1}$$

$$\mu\left(\frac{\partial n_B}{\partial t}+\mathbf{u}\cdot\nabla n_B\right)-\nabla\cdot\left(2\delta_B\left(\nabla n_B-\nabla\cdot\mathbf{B}\right)\right)=-c_B n_B^2+2c_A n_A, \tag{2}$$

$$\mu\overset{\triangledown}{\mathbf{A}} + \mathbf{A} - n_A\mathbf{I} - \nabla\cdot\delta_A\nabla\mathbf{A} = c_B n_B\mathbf{B} - c_A\mathbf{A}, \tag{3}$$

$$\epsilon\mu\overset{\triangledown}{\mathbf{B}} + \mathbf{B} - \frac{n_B}{2}\mathbf{I} - \nabla\cdot\epsilon\delta_B\nabla\mathbf{B} = -2\epsilon c_B n_B\mathbf{B} + 2\epsilon c_A\mathbf{A}, \tag{4}$$

wherein

$$\overset{\triangledown}{\mathbf{A}} = \frac{\partial\mathbf{A}}{\partial t} + \mathbf{u}\cdot\nabla\mathbf{A} - (\nabla\mathbf{u})^\top\cdot\mathbf{A} - \mathbf{A}\cdot\nabla\mathbf{u} \quad \text{and} \quad \overset{\triangledown}{\mathbf{B}} = \frac{\partial\mathbf{B}}{\partial t} + \mathbf{u}\cdot\nabla\mathbf{B} - (\nabla\mathbf{u})^\top\cdot\mathbf{B} - \mathbf{B}\cdot\nabla\mathbf{u} \tag{5}$$

are the upper-convected time derivatives of the chains conformational stress tensors, $\mathbf{u}$ is the solvent velocity and c_A, and c_B are the breakage and reforming rates of the long and short chains respectively. For the long chains, the breakage rate is given by $c_A = c_{Aeq} + c_{A,\dot\gamma}$, where c_{Aeq} is the equilibrium breakage rate, $c_{A,\dot\gamma} = \frac{1}{3}\xi\mu\left(2\mathbf{D} : \frac{\mathbf{A}}{n_A}\right)$ is the breakage rate dependent of the deformation rate, wherein $\mathbf{D} = \frac{1}{2}\left(\nabla\mathbf{u} + (\nabla\mathbf{u})^\top\right)$ is the strain rate tensor, and ξ is a parameter that define the degree of partial retraction of micelar structures. For the short chains, the reforming rate is constant and equal two the equilibrium value $c_B = c_{Beq}$.

It is interesting to note that the total number density of the chains is $n_T = 2n_A + n_B$. Using this expression, Eq. (1) and Eq. (2), we obtain the balance equation for n_T as

$$\mu\left(\frac{\partial n_T}{\partial t} + \mathbf{u}\cdot\nabla n_T\right) = \nabla\cdot 2\delta\nabla n_T - \nabla\nabla : 2\delta\left(\mathbf{A} + \mathbf{B}\right), \tag{6}$$

where the operator $\nabla\nabla$ is a second order tensor operator. Zhou *et al.* (2014) suggested that for the range $10^{-5} < \delta < 10^{-1}$ the terms $\nabla\nabla : \mathbf{A}$ and $\nabla\nabla : \mathbf{B}$ can be neglected in the number density equations. In this work, however, we show that this terms acts as source/sink terms and influence the flow behavior.

We have used the following relations in the evolution equations (here, the superscript * will be used to indicate dimensional variables):

$$\mathbf{x} = \frac{\mathbf{x}^*}{H},\ \ t = \frac{t^*}{\lambda_{eff}},\ \ \mathbf{u} = \frac{\lambda_{eff}\mathbf{u}^*}{H},\ \ p = \frac{p^*}{G_0},\ \ (\mathbf{A},\mathbf{B}) = \frac{H_A\left(\mathbf{A}^*,\mathbf{B}^*\right)}{G_0} \quad \text{and} \quad n_{A,B} = \frac{n^*_{A,B}}{n^{0*}_A}, \tag{7}$$

where H is the characteristic length of the geometry (channel width), λ_{eff} is the effective relaxation time of the network, G_0 is the elasticity modulus and n^{0*}_A is the equilibrium number density of long chains. The dimensionless breaking and reforming rates of the chains are given by,

$$c_A = \lambda_A c^*_A \quad \text{and} \quad c_B = \lambda_A n^{0*}_A c^*_B, \tag{8}$$

and

$$\mu = \frac{\lambda_A}{\lambda_{eff}}, \quad \epsilon = \frac{\lambda_B}{\lambda_A}, \quad \delta_A = \frac{\lambda_A D_A}{H^2} \quad \text{and} \quad \delta_B = \frac{\lambda_B D_B}{H^2}, \tag{9}$$

where μ is the ratio of the relaxation time of the long chains to the effective relaxation time of the network, ϵ is the ratio of the relaxation time of the short chains to the relaxation time of the long chains, δ_A and δ_B are the diffusion constants of the chains A and B, and D_A and D_B are the dimensional diffusion constants of the chains A and B.

The dimensionless momentum and mass conservation equations are given by

$$E^{-1}\left(\frac{\partial\mathbf{u}}{\partial t} + \mathbf{u}\cdot\nabla\mathbf{u}\right) = \nabla\cdot\left(-p\mathbf{I} + 2\beta\mathbf{D} + \mathbf{S_m}\right) \quad \text{and} \tag{10}$$

$$\nabla\cdot\mathbf{u} = 0, \tag{11}$$

where $E = De/Re = \lambda_{eff}\eta^*_0/\rho H^2$ represents the elasticity number, $De = \lambda_{eff}U^*/H$ is the Deborah number, $Re = \rho U^* H/\eta^*_0$ is the Reynolds number, U^* is the characteristic velocity, ρ is the density of the solution, p is the pressure, $\beta = \eta_s/\eta^*_0$ is the ratio of the solvent viscosity η_s and the micelles zero shear rate viscosity η^*_0. The micellar microestructure contribution in the stress is given by the dimensionless tensor,

$$\mathbf{S_m} = -\left(n_A + n_B\right)\mathbf{I} + \mathbf{A} + 2\mathbf{B}. \tag{12}$$

The balance equations Eq. (1) to Eq. (4), Eq. (10) and Eq. (11) must be supplemented with appropriated boundary and initial conditions.

We consider the same boundary conditions adopted by Kalb *et al.* (2017) e Kalb *et al.* (2018) for the cross-slot flow. Let $\mathcal{B}$ be a computational flow domain with boundary $\partial\mathcal{B}$ (Fig. 1). One portion of $\partial\mathcal{B}$, say $\mathcal{S}_i$, is the inlet flow boundary and, therefore, the following boundary conditions hold:

$$\mathbf{u} = -U\mathbf{n}, \quad n_A = n_A^0 \quad \text{and} \quad n_B = n_B^0, \quad \mathbf{A} = \mathbf{A}_{eq} \quad \text{and} \quad \mathbf{B} = \mathbf{B}_{eq} \quad \text{on} \quad \mathcal{S}_i, \tag{13}$$

where U is the uniform velocity, n_A^0, n_B^0, $\mathbf{A}_{eq}$ and $\mathbf{B}_{eq}$ are the number density and conformation tensors of the chains at the equilibrium, and $\mathbf{n}$ is the normal unit vector exterior to $\mathcal{S}_i$.

As for the outlet flow, we adopt zero traction and tangential velocity conditions, and zero flux of the number density and conformation tensors of the chains on $\mathcal{S}_o$, which is a complementary set of $\partial\mathcal{B}$:

$$(-p\mathbf{I} + 2\beta\mathbf{D})\,\mathbf{n} = \mathbf{0}, \quad \mathbf{u}\cdot\mathbf{t} = 0, \quad \mathbf{n}\cdot\nabla n_A = 0, \quad \mathbf{n}\cdot\nabla n_B = 0, \quad \mathbf{n}\cdot\nabla\mathbf{A} = \mathbf{0}, \quad \mathbf{n}\cdot\nabla\mathbf{B} = \mathbf{0} \quad \text{on} \quad \mathcal{S}_o, \tag{14}$$

where $\mathbf{t}$ is the tangential unit vector .

As for the impermeable wall, we assume

$$\mathbf{u} = \mathbf{0}, \quad \mathbf{n}\cdot\delta_A\left(2\nabla n_A - \nabla\cdot\mathbf{A}\right) = 0, \quad \mathbf{n}\cdot 2\delta_B\left(\nabla n_B - \nabla\cdot\mathbf{B}\right) = 0, \tag{15}$$

and

$$\mathbf{n}\cdot(\delta_A\nabla\mathbf{A}) = \mathbf{0}, \quad \mathbf{n}\cdot(\epsilon\delta_B\nabla\mathbf{B}) = \mathbf{0} \quad \text{on} \quad \mathcal{S}_w. \tag{16}$$

Note that $\mathcal{S}_i$, $\mathcal{S}_o$, and $\mathcal{S}_w$ are disjoint complementary sets of $\partial\mathcal{B}$, respectively.

The initial conditions of the problem are given by

$$\mathbf{u}_0 = \mathbf{0}, \quad n_A^0 = 1, \quad n_B^0 = \sqrt{\frac{2c_{Aeq}}{c_{Beq}}}, \quad \mathbf{A}_{eq} = \mathbf{I} \quad \text{and} \quad \mathbf{B}_{eq} = \frac{n_B^0}{2}\mathbf{I}. \tag{17}$$

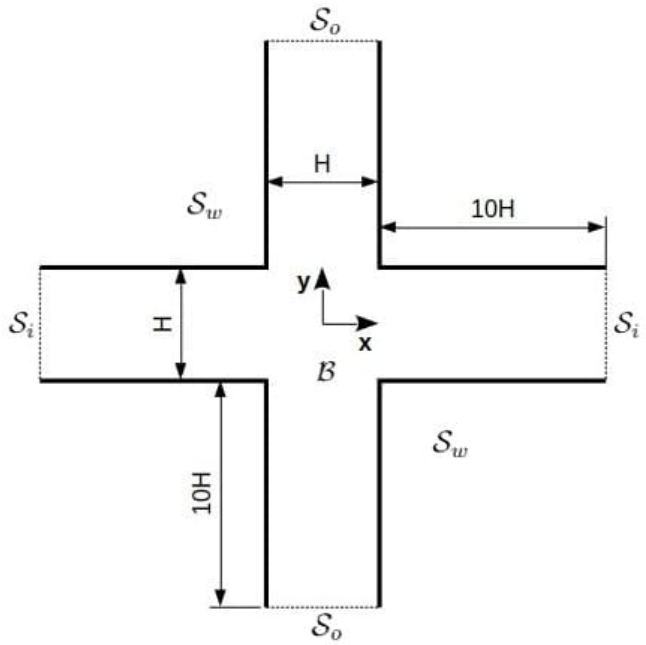

Figure 1: Cross-slot computational domain.

3. NUMERICAL APPROACH

The VCM model, Eq. (1) to Eq. (4), and the momentum and mass conservation equations, Eq. (10) and Eq. (11), were implemented and solved numerically using the finite element software COMSOL Multiphysics. We have adopted P_1-P_1 shape function for the velocity field and pressure with the Galerkin/least squares stabilization. We have used linear shape functions to approximate the stress tensors and the number density of the chains. The system of equations was discretized in time using a second order backward differentiation formulation (BDF). At each step time, the system of nonlinear equations was solved using the direct PARDISO solver. The solver was set up to recalculated the Jacobian matrix at each iteration.

The computational domain consists of four crossed channels, as shown in Fig. 1, with opposite inlets and outlets, which generate a stagnation point in the center of the geometry. The width and length of the channels have a ratio of 10:1, which ensure that the flow will arrive fully developed in the center of the geometry. To produce a small disturbance in the flow and allow the visualization of the symmetry break, we have used the same strategy adopted by Filali and Khezzar (2013) by introducing a very small distortion in the mesh topology, as indicate in Fig. 2.

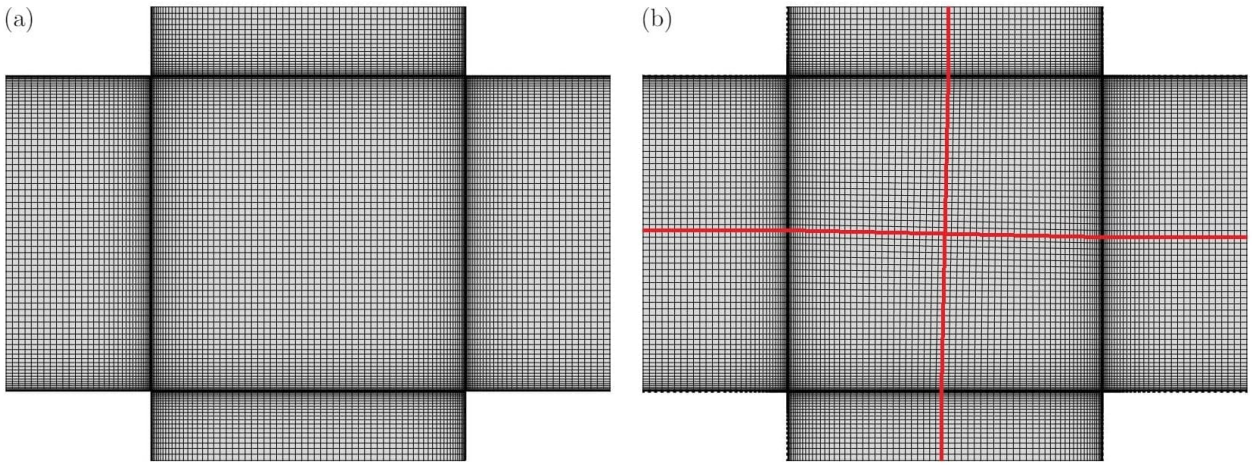

Figure 2: Detail of the mesh at the center of the cross-slot.

4. RESULTS AND DISCUSSION

In our simulations, we have adopted a wormlike micelle solution with the same rheological characteristics as that used by Kalb *et al.* (2018). The nondimensional parameters used in the VCM model are: $\beta = 1 \times 10^{-4}$, $\mu = 2.6$, $\epsilon = 5 \times 10^{-3}$, $\xi = 1 \times 10^{-2}$, $c_{Aeq} = 1.6$, $c_{Beq} = 0.8607$ and $\delta = \delta_A = \delta_B = 1 \times 10^{-2}$.

We present results for the velocity magnitude, $\|\mathbf{u}\|$, normalized by the maximum value of the velocity profile in the center of the inlet channels, $\|\mathbf{u}\|_{máx}$. The number density of long chains, n_A, normalized by the value in the equilibrium, n_A^0, and the principal stress difference, $\Delta\sigma = \sqrt{(T_{xx} - T_{yy})^2 + 4T_{xy}^2}$, normalized by the maximum, $\Delta\sigma_{máx}$.

Figures 3 to 5 show the results for the case where the source/sink term was neglected (i.e., $\nabla\nabla : [2\delta(\mathbf{A} + \mathbf{B})] = 0$) in Eq. (1) and Eq. (2). For low values of the Deborah number ($De = 0.30$), the flow remains perfectly symmetric, as shown in Fig. 3(a), with low changes in the number density of long chains, Fig. 4(a), and with high values of the principal stress difference in the extensional direction, due to the alignment of the long chains in that direction, Fig. 5(a). In Fig. 3(b), we observe that the flow remains symmetric for $De = 0.40$. However, the velocity field near the stagnation point undergoes a stretch in the direction of the exit channels. Due to the strong extensional flow near the stagnation point, the long-chain breakage intensifies in the direction of the exit channels, Fig. 4(b), as the principal stresses difference increases in this direction, Fig. 5(b). When De assume values higher than the value of the critical Deborah, $De = 0.45$, an elastic instability rises in the flow, leading to the loss of symmetry, Fig. 3(c). Due to the flow became asymmetrical, both the number density of long chains, as shown Fig. 4(c), and the principal stress difference, Fig. 5(c), assume asymmetrical configurations, with an intense breakage of the long chains in the corners due to the high principal stress difference in this region. For $De = 0.50$, the symmetry break in the flow field intensifies, Fig. 3(d), as well as the break of the long chains in the corners, as shown in Fig. 4(d), and the principal stress difference in that region, Fig. 5(d).

In Fig. 6 to 8, we show the results for the case where the source/sink term was considered (i.e., $\nabla\nabla : [2\delta(\mathbf{A} + \mathbf{B})] \neq 0$) in Eq. (1) and Eq. (2). When we consider this terms, the total number density of the chains is no longer constant and uniform, such effects were not accounted by Kalb *et al.* (2018). Comparing the results with and without the source/sink terms, we can notice that the interval where the De_{cr} is located was not modified. However, when we analyze the number density of long chains, we observe that the minimum value of n_A decreased, and the maximum value has exceeded the value of n_A at equilibrium, as shown Fig. 7, especially in the corners, which may have been a consequence of the high stresses in this region, Fig. 8. As the source/sink term depends on the chains confirmation, the total number density in a region increases or decreases according to the conformation of the species. In Fig. 9 we observe the distribution of the total concentration of chains in the central region of the cross-slot. In the case where we do not consider the term source/sink, the total concentration remains constant. When we consider this term, there is an increase in the total number density of the chains in the center, where the principal stress difference is higher.

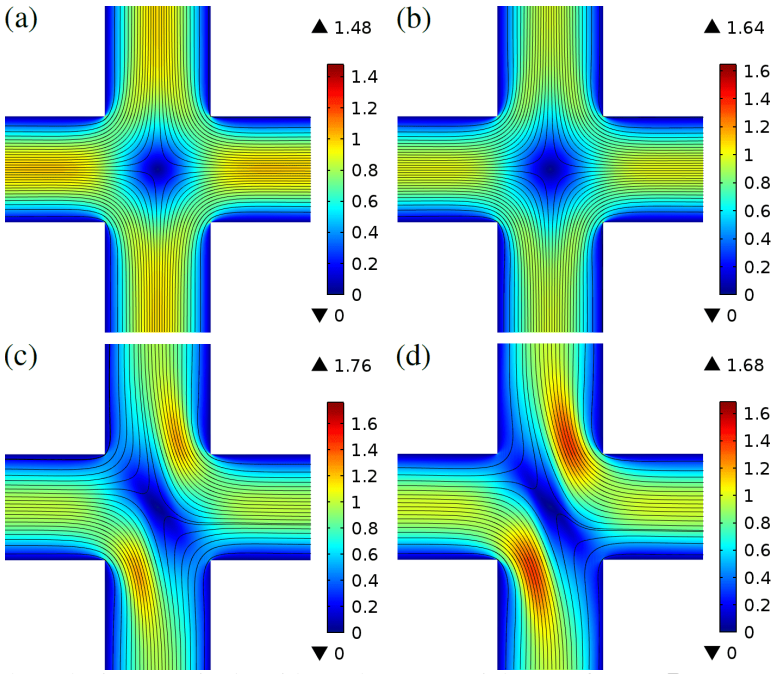

Figure 3: Contours of the velocity magnitude without the source/sink term for (a) $De = 0,30$, (b) $De = 0,40$, (c) $De = 0,45$ and (d) $De = 0,50$.

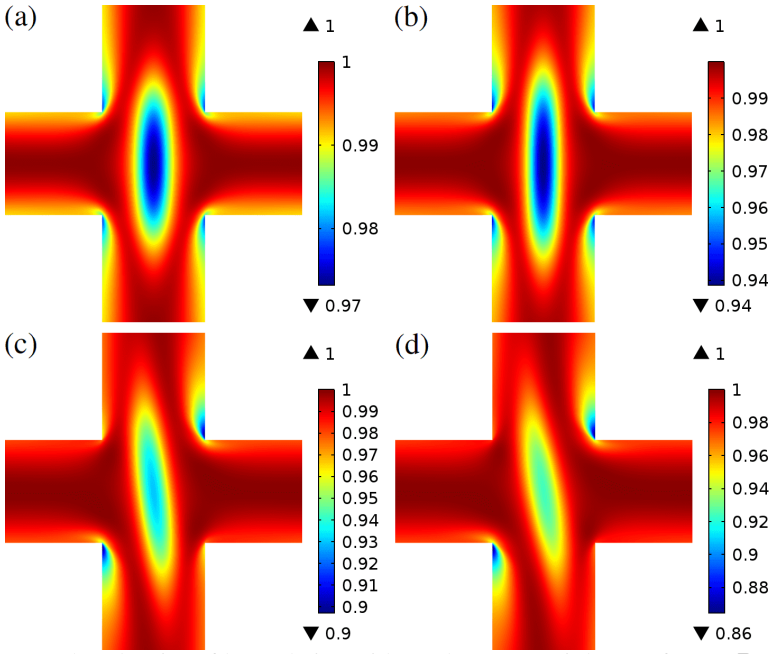

Figure 4: Contours of the number density of long chains without the source/sink term for (a) $De = 0,30$, (b) $De = 0,40$, (c) $De = 0,45$ and (d) $De = 0,50$.

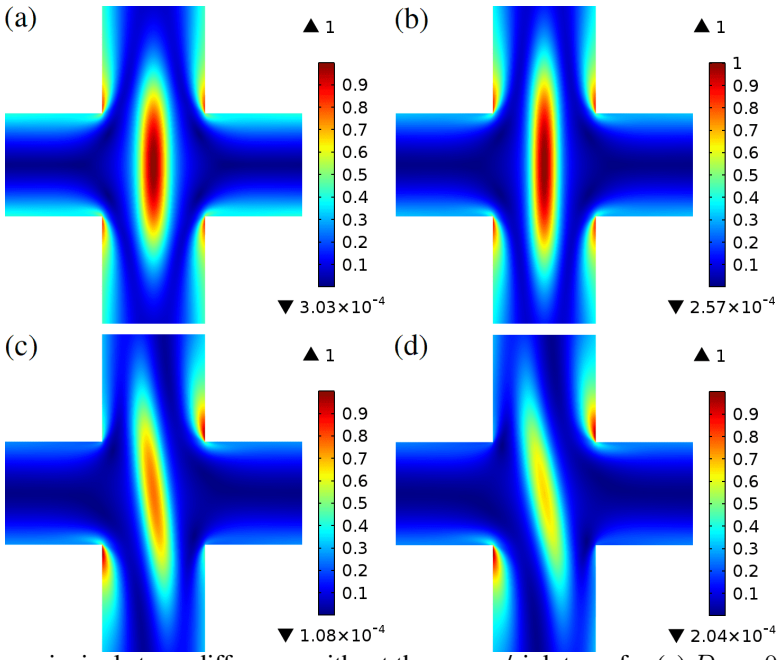

Figure 5: Contours of the principal stress difference without the source/sink term for (a) $De = 0,30$, (b) $De = 0,40$, (c) $De = 0,45$ and (d) $De = 0,50$.

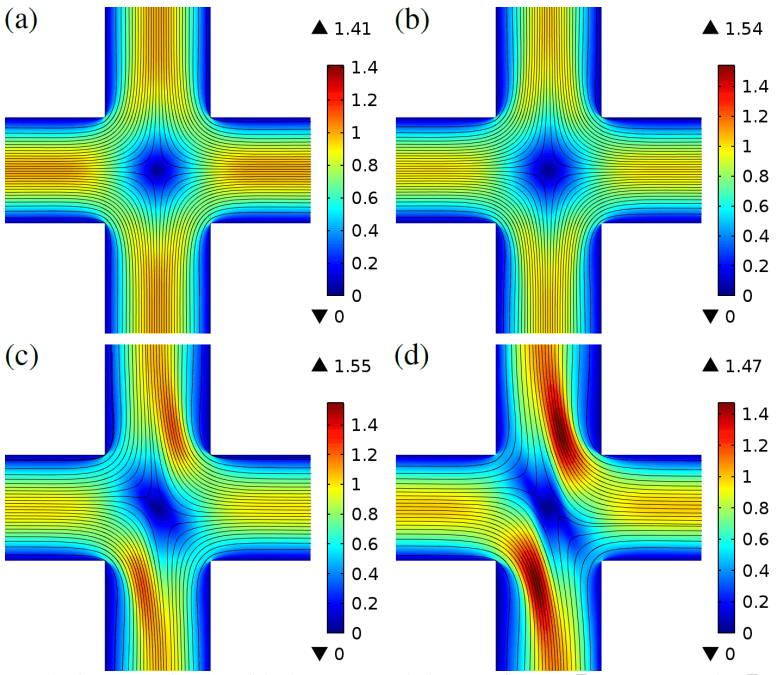

Figure 6: Contours of the velocity magnitude with the source/sink term for (a) $De = 0,30$, (b) $De = 0,40$, (c) $De = 0,45$ and (d) $De = 0,50$.

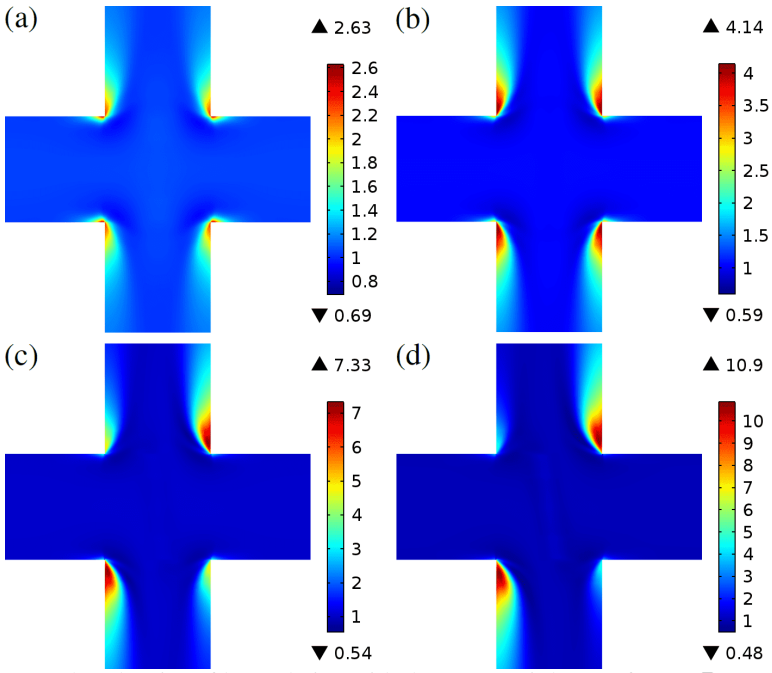

Figure 7: Contours of the number density of long chains with the source/sink term for (a) $De = 0,30$, (b) $De = 0,40$, (c) $De = 0,45$ and (d) $De = 0,50$.

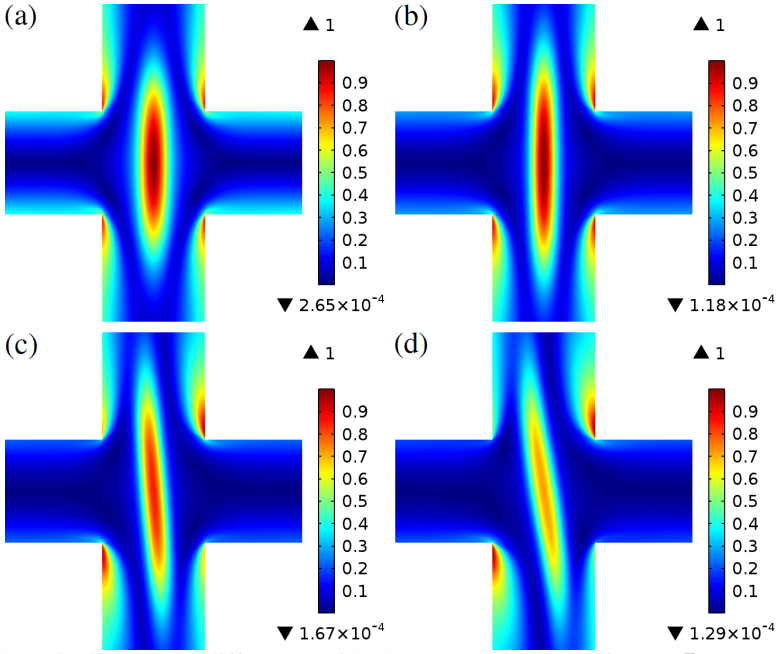

Figure 8: Contours of the principal stress difference with the source/sink term for (a) $De = 0,30$, (b) $De = 0,40$, (c) $De = 0,45$ and (d) $De = 0,50$.

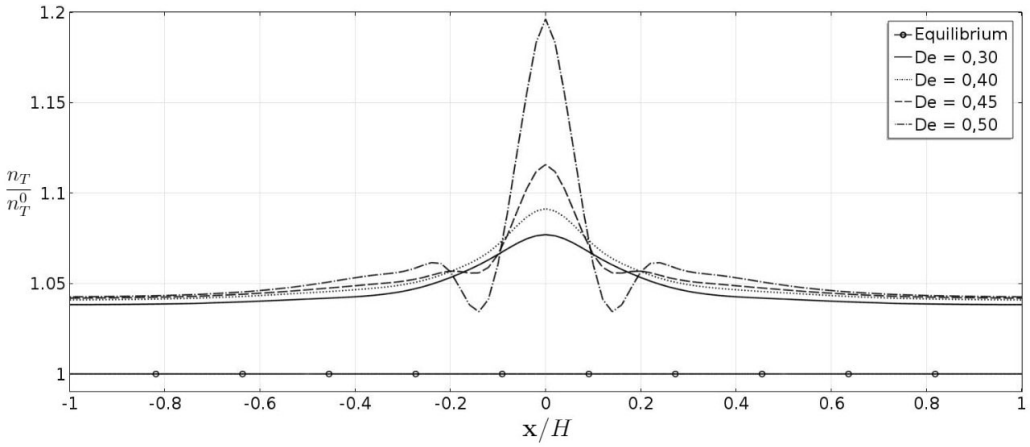

Figure 9: Total number density distribution, normalized by the equilibrium total number density (n_T/n_T^0), along the center line of the inlet channels (y = 0).

5. CONCLUDING REMARKS

We studied the phenomenon of purely elastic instability that occurs in micellar solution flows in a cross-slot geometry. The VCM model was chosen to describe the rheological behavior of the wormlike micelles. The model was implemented and solved using the finite element software COMSOL. The numerical results showed the symmetry breaking of the flow due to the elastic instability for a critical Deborah number. In the simulations we have carried out, we verify the influence of a source/sink terms presented in the balance equations for the number density of the chains, which have a strong influence on the total number density of the chains. This suggests that it should not be neglected in this type of analysis. However, further investigations are required.

6. ACKNOWLEDGEMENTS

This study was financed in part by the Coordenação de Aperfeiçoamento de Pessoal de Nível Superior - Brasil (CAPES) - Finance Code: 88881.200549/2018-01.

7. REFERENCES

Dubash, N., Cheung, P. and Shen, A.Q., 2012. "Elastic instabilities in a microfluidic cross-slot flow of wormlike micellar solutions". *Soft Matter*, Vol. 8, No. 21, pp. 5847–5856.

Filali, A. and Khezzar, L., 2013. "A finite element investigation of elastic flow asymmetries in cross-slot geometries using a direct steady solver". *FDMP: Fluid Dynamics & Materials Processing*, Vol. 9, No. 3, pp. 307–329.

Haward, S.J. and McKinley, G.H., 2012. "Stagnation point flow of wormlike micellar solutions in a microfluidic cross-slot device: Effects of surfactant concentration and ionic environment". *Physical Review E*, Vol. 85, No. 3, p. 031502.

Haward, S.J., Ober, T.J., Oliveira, M.S., Alves, M.A. and McKinley, G.H., 2012. "Extensional rheology and elastic instabilities of a wormlike micellar solution in a microfluidic cross-slot device". *Soft Matter*, Vol. 8, No. 2, pp. 536–555.

Kalb, A., Cromer, M. *et al.*, 2017. "Role of chain scission in cross-slot flow of wormlike micellar solutions". *Physical Review Fluids*, Vol. 2, No. 7, p. 071301.

Kalb, A., Villasmil-Urdaneta, L.A. and Cromer, M., 2018. "Elastic instability and secondary flow in cross-slot flow of wormlike micellar solutions". *Journal of Non-Newtonian Fluid Mechanics*.

Vasquez, P.A., McKinley, G.H. and Cook, L.P., 2007. "A network scission model for wormlike micellar solutions: I. model formulation and viscometric flow predictions". *Journal of non-newtonian fluid mechanics*, Vol. 144, No. 2-3, pp. 122–139.

Zhou, L., McKinley, G.H. and Cook, L.P., 2014. "Wormlike micellar solutions: Iii. vcm model predictions in steady and transient shearing flows". *Journal of Non-Newtonian Fluid Mechanics*, Vol. 211, pp. 70–83.

8. RESPONSIBILITY NOTICE

The authors are the only responsible for the printed material included in this paper.